# Phonon scattering between zero-dimensional electronic states: Spatial versus Landau quantization

U. Bockelmann
*Walter Schottky Institut, Technische Universität München, Am Coulombwall, D-85748 Garching, Germany*
(Received 2 May 1994)

Acoustic phonon scattering of electrons and excitons in fully quantized systems based on $GaAs/Ga_xAl_{1-x}As$ quantum wells is studied theoretically. We compare spatial quantization by lateral potentials (quantum dots) with Landau quantization by a magnetic field. In the Born approximation, the rate of electron scattering from the first excited state to the ground state of a parabolic quantum dot is one-half of the corresponding transition rate between Landau levels. When an increasing magnetic field is applied to a dot of sizable lateral confinement, the scattering rate first increases strongly, then exhibits pronounced oscillations, and finally decreases at high fields. Exciton relaxation by phonon emission is enhanced by a magnetic field in this system. The relaxation dynamics of quantum dot excitons strongly differs from that of magnetoexcitons in quantum wells.

## I. INTRODUCTION

The characteristic electronic structure of crystals consists of energy bands with a quasicontinuous spectrum seperated by energy gaps. Deviations from the periodicity caused by defects or impurities may lead to discrete, electronic states within the gaps of the bulk band structure. Artificial structures on the other hand, allow us to transform the energy bands of the solid into a ladder of discrete levels in a controlled way, at least in principle. Examples of this kind of quasi-zero-dimensional (0D) systems are quantum dots defined by imposing lateral confinement in the 2D plane of semiconductor quantum wells either directly during epitaxial growth or subsequently by a lateral patterning technique.[1] In an alternative way, complete quantization can be obtained by applying a magnetic field perpendicular to the 2D plane of the quantum well (Landau quantization).

The interaction between electronic states and lattice vibrations in low-dimensional semiconducor structures has been widely studied.[2] In quantum dots, where complete spatial confinement induces a discrete energy spectrum, electron-phonon scattering is strongly modified with respect to systems of higher dimensionality.[3] Scattering by longitudinal optical (LO) phonons, which in III-V compounds represent the dominant mechanism of thermalization between electronic states and the lattice, is possible only when the energy separation between initial and final state is of the order of the LO-phonon energy, which, in general, is difficult to achieve in a quantum dot. Longitudinal acoustic- (LA-) phonon scattering becomes inefficient when the splitting between the 0D levels exceeds a threshold value depending on the smallest dimension of the structure (typically some meV for quantum dots fabricated from quantum wells). Benisty *et al.* have pointed out that the resulting slow relaxation of excited electrons down into the ground state can give rise to an intrinsic limitation of the luminescence efficiency of 0D semiconductor structures.[4] It is, however, difficult to suppress efficient relaxation of excited carriers, in general, since there are a number of possible relaxation mechanisms. Recently, the importance of two-phonon scattering,[5] of Auger processes,[6] and of excitonic effects[7] have been studied theoretically. Indications for a slowed energy relaxation have been observed in photoluminescence experiments on single GaAs quantum dots.[8] The other limiting case, scattering between purely Landau quantized states, has been discussed,[9–12] in particular, in the context of the breakdown of the quantum Hall effect.

In the present paper, we compare the effect of complete spatial quantization on electron and exciton relaxation with the one of Landau quantization. The outline is as follows. In Sec. II A we introduce the energies and wave functions of electrons in a parabolic quantum dot in magnetic field. In Sec. II B results on electron-LA-phonon scattering are presented, including a discussion of the gradual transition from spatial quantization to Landau quantization. The exciton case is treated in Sec. III. Section IV contains the conclusions.

## II. ELECTRONS IN PARABOLIC DOTS AND MAGNETIC FIELD

### A. Energies and wave functions

We consider structures based on $GaAs/Ga_{0.7}Al_{0.3}As$ quantum wells. An envelope function description of the electronic states in a one band effective mass approximation is employed. It is assumed that the confinement by the quantum well grown along the $z$ axis is much stronger than the lateral confinement. This facilitates the problem since the effective-mass Hamiltonian can, to a good

 

approximation, be written as[13]

$$H = H_{xy} + H_z \ . \tag{1}$$

The lateral motion is decoupled from the one along $z$ and the envelope functions separate $\psi(\mathbf{r}) = \phi(\vec{r})\chi(z)$ (arrows indicate 2D vectors defined in the $xy$-plane, boldface 3D vectors). The $z$-dependent part $\chi$ is an eigenfunction of the quantum well Hamiltonian,

$$H_z = \frac{-\hbar^2}{2}\partial_z \frac{1}{m^*(z)}\partial_z + V_c\Theta\left(|z| - \frac{L_z}{2}\right) \ . \tag{2}$$

$V_c$ is the offset between the band edges of the well and the barrier ($\theta$ is the Heavyside function) and $m^*(z)$ the $z$-dependent effective mass. Throughout the paper, we assume carriers in the ground state of the quantum well of width $L_z$.

Along the lateral directions, we consider the Hamiltonian

$$H_{xy} = \frac{(\vec{p} - \vec{A}Q)^2}{2m} + \frac{1}{2}m\omega_0^2 r^2 \ , \tag{3}$$

where we have used the symmetrical gauge $\vec{A} = (-y, x)B/2$ to relate the vector potential to a magnetic field $B$ applied along the $z$ axis. An $\vec{r}$-independent lateral effective mass $m = m^*(z = 0)$ is assumed and the electron charge $Q = -e$ is introduced. Lateral spatial confinement is modeled by a parabolic potential with rotational symmetry in the $xy$ plane. $H_{xy}$ is the Hamiltonian of a 2D harmonic oscillator in a perpendicular magnetic field which has an analytical solution.[14] The wave functions, parametrized by the radial quantum number $n$ (0,1,2,...,) and the angular quantum number $l$ ($0, \pm1, \pm2, \ldots,$), are

$$\phi_{n,l}(\vec{r}) = \left(\frac{n!}{\pi\alpha^2\,(n + |l|)!}\right)^{1/2} \rho^{|l|} L_n^{|l|}\left(\rho^2\right) e^{-\rho^2/2} e^{-il\varphi} \ . \tag{4}$$

The lateral position vector is expressed in polar coordinates as $\vec{r} = \rho\alpha\,(\cos\varphi, \sin\varphi)$ with $\omega_c = eB/m$, $\omega = \sqrt{\omega_0^2 + \omega_c^2/4}$, and $\alpha = \sqrt{\hbar/(m\omega)}$. The Laguerre polynomials $L$ are defined in accordance with Ref. 15. The corresponding energy spectrum is given by

$$E_{n,l} = (2n + |l| + 1)\hbar\omega - \frac{1}{2}\hbar\omega_c l \ . \tag{5}$$

It is convenient to introduce the dimensionless quantities $\lambda = \omega_c/(2\omega)$ and $\epsilon = E_{n,l}/(\hbar\omega)$ to discuss the gradual transition from pure spatial quantization ($\omega_0 > 0, \omega_c = 0, \lambda = 0$) to pure Landau quantization ($\omega_0 = 0, \omega_c > 0, \lambda = 1$). Equation (5) transforms into

$$\epsilon = (2n + |l| + 1) - l\lambda \ . \tag{6}$$

In this representation the energy spectrum consists of a set of straight lines, shown in Fig. 1. Each state $\phi_{n,l}$ corresponds to one line with a slope given by $-l$. For $l \geq 0$, the quantum number $n$ determines the intersection with the vertical axis $\lambda = 1$. At $\lambda$=0, the degeneracy is equal to $\epsilon$, while at $\lambda$=1 we obtain the well known, macroscopic degeneracy of Landau levels. Figure 1 is limited to states of angular momentum $l \leq 10$, otherwise there would be an infinite number of lines (for an infinite sample area) of increasing slope arising from each of the levels at $\lambda = 1$. Between the two limiting cases, there are many level crossings. Following the state ($n = 0, l = -1$), an example which is used in Sec. II B, crossings with states of ($n = 0, l > 0$) occur at $\lambda = (l - 1)/(l + 1)$.

### B. Electron scattering by LA phonons

In this section, scattering between the discrete electron states is considered. We study the interaction with bulk phonons of the well material. The presence of heterointerfaces along the growth direction and eventually along lateral directions is neglected as far as the phonon modes are concerned. Roughly speaking, this is based on the fact that the lattice ions are much heavier than the electrons and, therefore, quantum confinement energies of phonons are weak compared to electron ones[16]. The bulk phonon approximation is expected to work well for low-dimensional systems that are embedded pseudomorphically in a semiconductor matrix which act as a barrier for the electronic states but exhibit similar lattice properties as the well, wire or dot material itself. The bulk optical phonon dispersions of GaAs and AlAs do not overlap in energy which leads to the presence of confined and interface modes for the optical phonons in GaAs/$Ga_xAl_{1-x}$As heterostructures. Nevertheless, recent calculations of the electron-optical phonon interaction based on a microscopic description of the phonons show that the assumption of unmodified bulk phonon modes provides reasonable results for the total scattering rates in GaAs/AlAs quantum wells and wires[17,18]. Acoustic modes are much less affected since the acoustic branches overlap in energy leading to phonon modes which are propagative throughout the structure and therefore remain bulklike. Some 0D structures are fabricated by etching through a quantum well, thus exhibiting free surfaces. But as these structures are quite big (typically several hundreds of angstroms) compared to the lattice unit cell the electron-LA-phonon scattering is again well described within the bulk phonon approximation. The situation is different in II-VI semiconductor microcrystals.[19] There a large portion of the atoms are related to the crystal surface and, therefore, all phonon modes and the electron-phonon coupling can be significantly different as compared to the bulk.

Energy conservation requires that the interacting phonon corresponds to the energy separation of the initial and final electron states. LO-phonon scattering is widely suppressed in 0D structures, due to the discrete electronic energy spectrum together with the small LO-phonon energy range. We, therefore, consider the interaction with longitudinal acoustic (LA) phonons. Phonon scattering rates are calculated from the Fermi golden rule,

$$\tau_{i\to f}^{-1} = \frac{2\pi}{\hbar}\sum_{\mathbf{q}} |\langle\psi_f|W|\psi_i\rangle|^2 \delta\left(E_f - E_i \pm E_q\right) \times \left[n_B\left(E_q, T_l\right) + \frac{1}{2} \pm \frac{1}{2}\right], \quad (7)$$

where the interaction operator $W$, in terms of the electron-phonon formfactor $\Lambda(q)$, is given by

$$W = \Lambda(q) e^{\mp i\mathbf{q}\cdot\mathbf{r}} \quad (8)$$

The upper (lower) case accounts for emission (absorption) of phonons by an electron in the initial state $\psi_i$. The sum extends over all phonon wave vectors $\mathbf{q}$. It is assumed that the initial (final) electron state is occupied (unoccupied). The thermal occupation of phonons of energy $E_q$ at the lattice temperature $T_l$ is given by the Bose-Einstein distribution $n_B$. The coupling of electrons to LA phonons by means of a deformation potential $D$ is described by

$$\Lambda_{e-LA}(q) = \sqrt{\frac{\hbar q}{2\rho c_s}} D \ , \quad (9)$$

assuming an isotropic phonon dispersion $\omega_q = c_s q$. We use the GaAs parameters $\rho = 5300$ kg/m$^3$, $c_s = 3700$ m/s and $D = 8.6$ eV. Piezoelectric coupling to acoustic phonons exists in the present system, but is found to be an order of magnitude weaker than the deformation potential interaction in experiments on 2D GaAs/$Ga_xAl_{1-x}As$ structures.[20,21] The Hamiltonian of the piezoelectric interaction is of the form Eq. (8), with a different formfactor $\Lambda$. Qualitatively, the results for deformation potential interaction also apply to piezoelectric coupling since the important part is the harmonic exponential. For the electron states given above, the relevant matrix element is

$$\langle\psi_i | e^{i\mathbf{q}\mathbf{r}} | \psi_f\rangle = f_{xy}(\vec{q}) F_z(q_z L_z/2) \ . \quad (10)$$

For an infinite barrier ($V_c \to \infty$) quantum well holds:[22]

$$F_z(x) = \frac{\sin x}{x}\left(\frac{1}{1 - x^2/\pi^2}\right) \ . \quad (11)$$

This expression shows that the squared matrix element strongly decreases for $q_z > 2\pi/L_z$. This reflects a general feature of electron-phonon interaction: Coupling is weak when along a given direction the phonon wavelength is small compared to the spatial variation of the electron wave function. In the numerical calculations we use, instead of Eq. (11), an expression which takes the finite-barrier height into account.[23] The phonon wave vector written in spherical coordinates $\mathbf{q} = q(\cos\varphi \sin\vartheta, \sin\varphi \sin\vartheta, \cos\vartheta)$, it follows for the lateral matrixelement:

$$f_{xy}(\vec{q}) = \langle n, l | e^{i\vec{q}\cdot\vec{r}} | n', l'\rangle = e^{i(l-l')(\varphi+\pi/2)} G(\alpha q \sin\vartheta, n, l, n', l'), \quad (12)$$

with

$$G(Q, n, l, n', l') = 2\left(\frac{n! n'!}{(n+|l|)!(n'+|l'|)!}\right)^{1/2} \times \int_0^\infty dx x^{|l|+|l'|+1} e^{-x^2} \times L_n^{|l|}\left(x^2\right) L_{n'}^{|l'|}\left(x^2\right) J_{l-l'}(Qx) \ . \quad (13)$$

Substitution of Eqs. (8)–(13) into Eq. (7) gives

$$\tau_{i\to f}^{-1} = \frac{D^2 q_0^3}{4\pi\rho\hbar c_s^2}\left[n_B\left(\hbar c_s q_0, T_l\right) + \frac{1}{2} \pm \frac{1}{2}\right] \times \int_0^{\pi/2} d\vartheta \sin\vartheta \, G^2(\alpha q_0 \sin\vartheta, n_i, l_i, n_f, l_f) \times F_z^2(q_0 \cos\vartheta L_z/2) \ , \quad (14)$$

where $q_0 = |E_i - E_f|/(\hbar c_s)$. Equation (14) describes LA-phonon scattering of electrons in the presence of spatial lateral confinement and (or) magnetic field. For a given transition $i \to f$, the ratio of the lateral confinement length $\alpha$ and the phonon wavelength $\lambda_q = 2\pi/q_0$ determines the lateral matrixelement $G$ and the product $q_0 L_z$ governs $F_z$. To illustrate the essential features contained in Eq. (14), we discuss two examples: (1) scattering from the $(n = 0, l = 1)$ state and (2) scattering from the $(n = 0, l = -1)$ state, both at zero temperature. At $\lambda = 0$, these initial states are degenerate and correspond to the first excited quantum dot level ($\epsilon = 2$ in Fig. 1). As magnetic field increases initial state 1 evolves towards the lowest Landau level [from $(\lambda, \epsilon)$=(0,2) $\to$ (1,1) in Fig. 1]. State 2 goes to the first excited Landau level [(0,2) $\to$ (1,3)], through many level crossing as mentioned in Sec. II A. For these transitions, the lateral matrix elements can be expressed in closed form

$$G(Q, 0, -1, 0, l') = l'!^{-1/2}\left(-\frac{Q}{2}\right)^{l'+1} e^{-Q^2/4} \ . \quad (15)$$

$G^2$ exhibits a maximum at $Q = \sqrt{2(l'+1)}$.

In Figs. 2–5, we present numerical results for electrons in 0D systems based on GaAs/$Ga_{0.7}Al_{0.3}As$ quantum wells. At $B$=0, the rates of scattering from initial

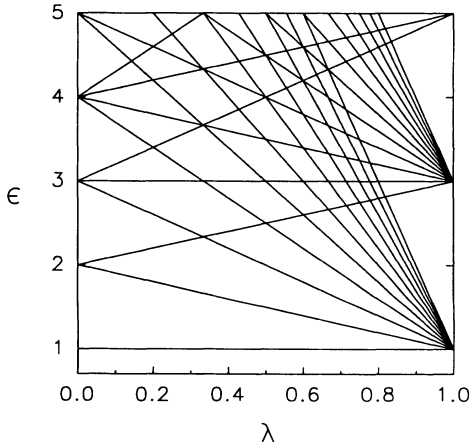


FIG. 1. Single-particle energy spectrum according to Eq. (6).

state 1 and 2 are equal, since the states are degenerate and $G^2(Q,0,1,0,0) = G^2(Q,0,-1,0,0)$. Due to energy conservation all emitted LA phonons have the same energy $E_q = \hbar\omega_0$. Figure 2 shows that in a parabolic quantum dot the scattering rate first increases with lateral confinement, passes a maximum, and strongly decreases for large $\omega_0$. The increase at small $\omega_0$ is caused by the $q$ dependence of the deformation potential form factor [Eq. (9)]. For large $\omega_0$ the phonon wavelength becomes smaller than the smallest dimension of the quantum dot ($\lambda_q < L_z$) and the scattering rate decreases by orders of magnitude. The same behavior has been found for quantum dots with square shaped lateral potentials of infinite barrier height.[3,4] The mean angle $\langle\vartheta\rangle$ of the emitted LA phonons (right axis) is obtained by multiplying the integrand of Eq. (14) by $\vartheta$ and dividing the final result by $\tau^{-1}_{i\to f}$. Starting from a value of 7/6 at small phonon energy, the mean angle continuously decreases with increasing $\omega_0$. The small energy limit of $\langle\vartheta\rangle$ depends on the quantum numbers of the initial and final states, but not on the dot dimensions. This follows directly from a development of $F_z$ and $G$ for small arguments. For large $\omega_0$, the phonon emission is highly anisotropic. It is oriented along the direction of strongest confinement, here the quantum well growth axis $z$.

A fundamental difference between spatial and Landau quantization is the macroscopic degeneracy of the Landau levels (the number of states per Landau level is proportional to the sample area). Elastic as well as inelastic scattering mechanisms lead to a Landau level broadening and a mixing of the degenerate eigenstates. To calculate scattering rates in this system, one has to take into account the broadening effects self-consistently.[24] Elastic scattering (e.g., interface roughness and impurity scattering) strongly contribute to the broadening of Landau levels, in particular in narrow quantum wells, and thus have to be included in a self-consistent calculation. As a consequence, the scattering rates are sample dependent. In this work, we consider scattering between states whose energy difference is large compared to the Landau level broadening. In this limit the details of the elastic scattering mechanisms which are difficult to quantify should be less important. The hope is that the scattering rates, calculated between unperturbed eigenstates in the Born approximation, still contain the essential physical features of the full, much more complex problem.

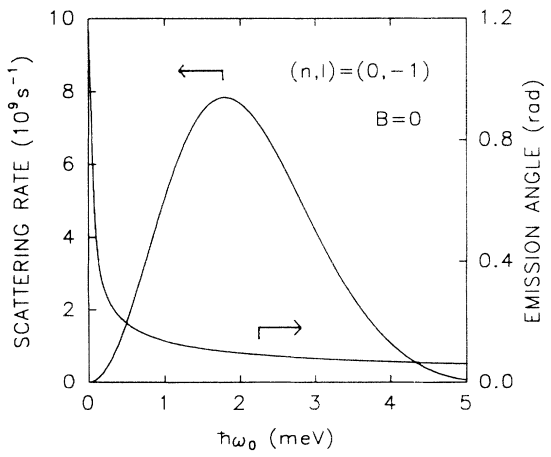


FIG. 2. Rate $\tau^{-1}$ and mean phonon emission angle $\langle\vartheta\rangle$ for scattering from the first excited electron state of a quantum dot, as a function of the lateral confinement. According to Eq. (16) the curves also apply to scattering between Landau levels. GaAs/$Ga_{0.7}Al_{0.3}As$, $L_z = 3$ nm, $T_l = 0$.

At $\lambda = 1$ an electron in initial state 2 has a macroscopically degenerate final state available at lower energy, while at $\lambda = 0$ there is only the nondegenerate quantum dot ground state. We now show that the total scattering rate from the state in the first excited Landau level is simply related to the case of pure spatial confinement. Let us compare $\lambda$=0 and 1 for the same energy difference between the first excited and the ground state ($\omega_0 = \omega_c$). It follows $q_0^{(\lambda=1)} = q_0^{(\lambda=0)}$ and $\alpha^{(\lambda=1)} = \sqrt{2}\alpha^{(\lambda=0)}$. Therefore, the differences in Eq. (14) amount to the use of $\sum G^2(\sqrt{2}Q,0,-1,0,l')$ instead of $G^2(Q,0,-1,0,0)$. From Eq. (15) follows

$$\sum_{l'=0}^{\infty} G^2(\sqrt{2}Q,0,-1,0,l') = \sum_{l'=0}^{\infty} l'!^{-1}\left(\frac{Q}{\sqrt{2}}\right)^{2l'+2} e^{-Q^2}$$
$$= 2\frac{Q^2}{4}e^{-Q^2/2}$$
$$= 2G^2(Q,0,-1,0,0)\ . \qquad (16)$$

This shows that the scattering rate between the Landau states is twice the one between the quantum dot levels. The angle distribution of the emitted phonons is the same. We should keep in mind that the factor of 2 correspondance between the scattering rates is derived only for the initial state ($n = 0, l = -1$) and not for the other degenerate states belonging to the first excited Landau level.

In Fig. 3, we present the $B$-field dependence of the rate and the mean emission angle for scattering from initial state 1. The phonon energy $E_q$, given in the upper horizontal scale, decreases homogeneously with increasing $B$, most strongly for $\omega_c < \omega_0$ (below 2 T). The peak in $\tau^{-1}$ near 5 T reflects the maximum in the lateral matrixelement $G$. At higher fields, the scattering rate decreases and $\langle\vartheta\rangle$ approaches the small energy limit 7/6 of this transition. The results presented in Figs. 2 and 3 are easily generalized to finite temperatures. Since all interacting phonons have the same energy, we just need to multiply the total scattering rate by the phonon occupation number given by the square bracket in Eq. (14).

Results for scattering from initial state 2 are given in Fig. 4 ($\hbar\omega_0 = 2$ meV) and Fig. 5 ($\hbar\omega_0 = 6$ meV). A sum over all available final states has been performed. Scattering rate $\tau^{-1}$, mean phonon energy $\langle E_q\rangle$ and emission angle $\langle\vartheta\rangle$ show pronounced magnetic field oscillations. This is caused by the level crossings of the initial state discussed above. Each time a new final state becomes available, $\tau^{-1}$ and $\langle\vartheta\rangle$ exhibit a peak while $\langle E_q\rangle$ shows a sudden decrease. The oscillations are damped with increasing $B$ since the angular momentum quantum numbers of the initial and final states become increasingly different.

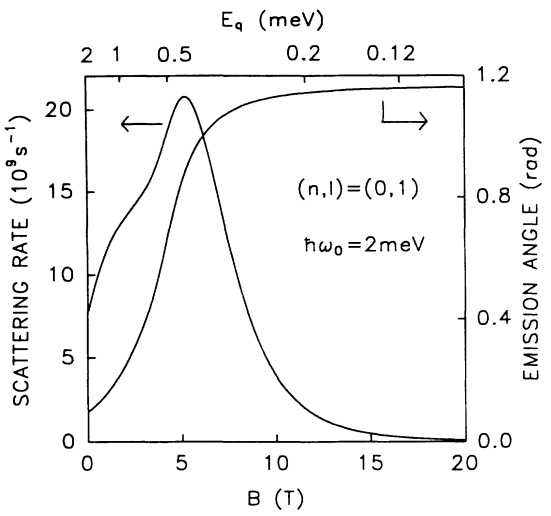


FIG. 3. Rate $\tau^{-1}$ and mean emission angle $\langle\vartheta\rangle$ for scattering from the $(n = 0, l = 1)$ electron state of a quantum dot as a function of magnetic field. The corresponding phonon energy $E_q = \hbar(\omega - \omega_c/2)$ is given on the upper scale. $GaAs/Ga_{0.7}Al_{0.3}As$, $L_z = 3$ nm, $T_l = 0$.

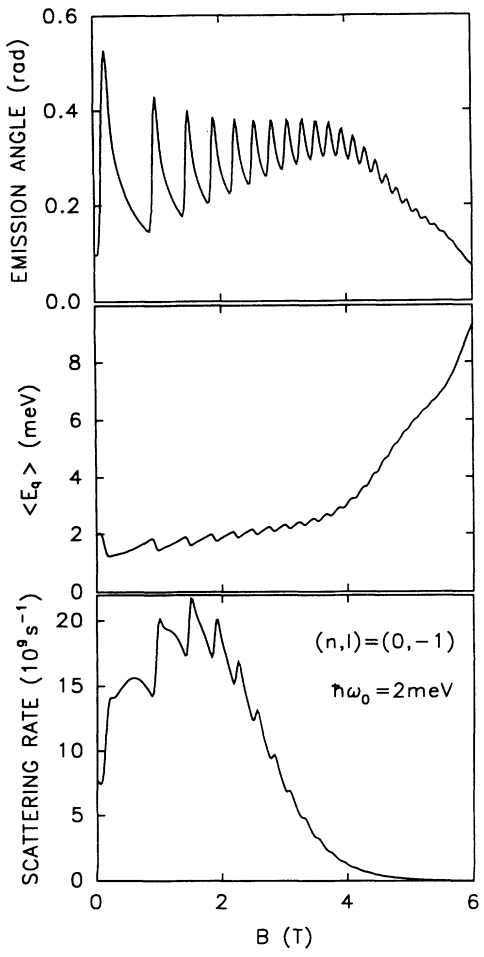


FIG. 4. Scattering rate $\tau^{-1}$, mean phonon energy $\langle E_q\rangle$, and mean emission angle $\langle\vartheta\rangle$ for scattering from the $(n = 0, l = -1)$ electron state. $GaAs/Ga_{0.7}Al_{0.3}As$, $L_z = 3$ nm, $T_l = 0$.

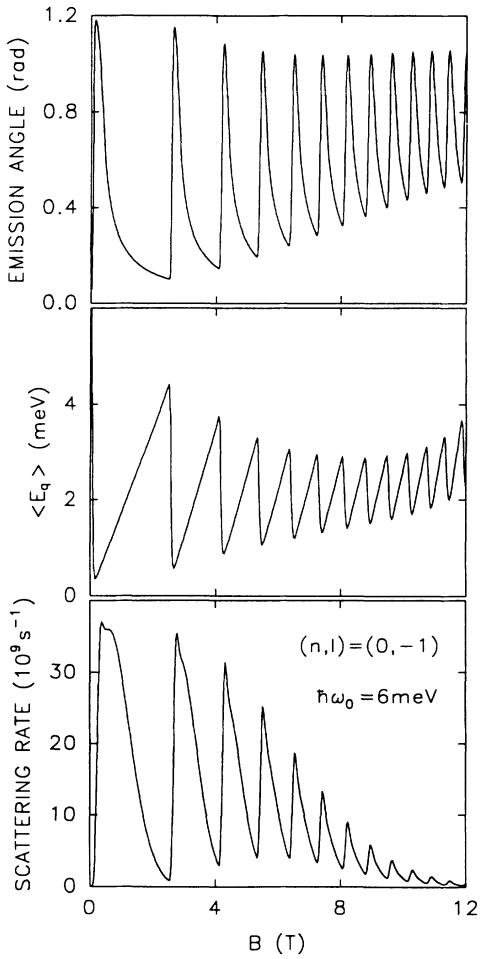


FIG. 5. As Fig. 4 for $\hbar\omega_0 = 6$ meV.

Concluding this section, the electron-LA-phonon interaction is to a large extent determined by the interplay of three lengths: the lateral confinement length $\alpha$, the quantum well width $L_z$, and the phonon wavelength $\lambda_q = 2\pi/q_0$. As long as the latter is much smaller than $\alpha$ and $L_z$ scattering is weak. Strong variations in $\tau^{-1}$ occur when $\lambda_q$ is commensurable with $\alpha$ and (or) $L_z$.

## III. QUANTUM DOT EXCITONS AND MAGNETOEXCITONS

Similar to the electron case considered above, we construct the exciton states on the ground conduction and valence subbands of the quantum well underlying the 0D system. Heavy-hole–light-hole (hh-lh) mixing and the contribution of excited subbands are neglected for the sake of simplicity. This approximation can be justified only as long as the splitting between the hh and lh ground states and the confinement energies of excited subbands are large compared to the lateral confinement energies and the exciton binding energy. Therefore, in the numerical calculations, we restrict ourselves to systems based on a narrow GaAs quantum well ($L_z = 3$ nm). For magnetoexcitons in GaAs quantum wells of width above 10 nm

it has been shown that hh-lh mixing is important.[25,26] To describe the exciton motion in the $xy$ plane, we consider the Hamiltonian:

$$H = H_e + H_h + H_{\rm int}. \tag{17}$$

$H_e$ and $H_h$ are given by Eq. (3) with the appropriate parameters for electrons and heavy holes. The parabolic lateral potentials ($1/2m_e\omega_{0,e}^2 r_e^2$ and $1/2m_h\omega_{0,h}^2 r_h^2$) confine electron and hole at the same spatial position. We neglect the spin splitting in the conduction and valence band. The Coulomb interaction is described by

$$H_{\rm int}(|\vec{r}_e - \vec{r}_h|) = -\frac{2\pi e^2}{\kappa}\sum_{\vec{q}}\frac{f_z(q)}{q}e^{i\vec{q}\cdot(\vec{r}_e-\vec{r}_h)}, \tag{18}$$

with the form factor

$$f_z(q) = \int dz \int dz' e^{-q|z-z'|}\,|\chi_e(z)|^2\,|\chi_h(z)|^2 \ .$$

The envelope functions $\chi_e$ and $\chi_h$ are the electron- and heavy-hole ground state wave functions of the quantum well [Eq. 2]. A spatially constant, static dielectric funtion $\kappa = 4\pi\epsilon_0\epsilon_s$ ($\epsilon_s = 12.9$) is used. The electron-hole exchange interaction is neglected. For spherical quantum dots, the effect of dielectric confinement and the exchange interaction has been discussed by Takagahara.[27] We use the following expansion of the exciton envelope function:

$$\psi_{\rm ex}^j(\mathbf{r}_e,\mathbf{r}_h) = \chi_e(z_e)\chi_h(z_h)\sum_{n_e,n_h,l_e} c_{j,n_e,n_h,l_e} \times\phi^e_{n_e,l_e}(\vec{r}_e)\phi^h_{n_h,j-l_e}(\vec{r}_h). \tag{19}$$

The analytical basis functions $\phi$ are given by Eq. (4). Due to the rotational symmetry around the $z$ axis, the total angular momentum $j = l_e + l_h$ is a good quantum number and the development is restricted to $n_e$, $n_h$, and $l_e$. The Hamiltonian $H$ is numerically diagonalized after an expansion on the basis Eq. (19).

In Fig. 6, the energies of the lowest $j = 0$ exciton states are presented as a function of magnetic field. Only excitons with $j = 0$ can decay radiatively by an allowed interband transition.[28] The radiative decay rate, given by the horizontal bars, is calculated from the exciton wave function using Eq. (4) of Ref. 7. The energies of the lowest nonradiative ($j \neq 0$) exciton states are presented in Figs. 7,8. The exciton binding energy $\langle\psi_{\rm ex}| - H_{\rm int}|\psi_{\rm ex}\rangle$ increases with magnetic field, similar to the case of quantum well excitons.[29] The binding energy of the ground state exciton, for instance, goes from 13.2 meV at zero field to 18 meV at 15 T.

The expansion in terms of single-particle solutions has been employed in most theoretical studies of excitons in semiconductor quantum dots.[30–33] It converges rapidly only for strong lateral confinement. For Figs. 6–9, we have used the 300 lowest energy basis states for each value of $j$. In this regime of weak lateral confinement the basis states are strongly mixed by the Coulomb interaction term $H_{\rm int}$. An alternative way consists of rewriting $H$ in terms of center of mass (c.m.) and relative coordinates:[33,34]

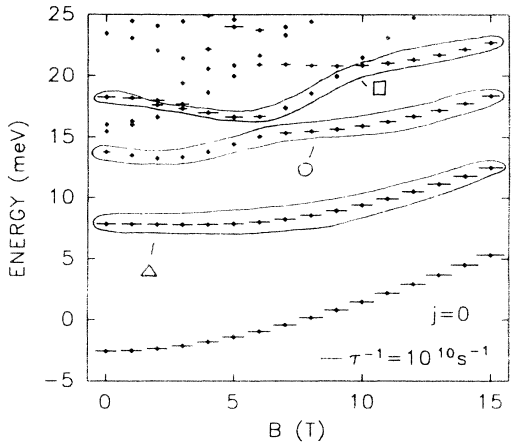


FIG. 6. Magnetic field dispersion of the lowest excitons of zero-angular momentum $j$ for a quantum dot with $\hbar\omega_{0,e} = 6$ meV; $\hbar\omega_{0,h} = 4.7$ meV based on a GaAs/$Ga_{0.7}Al_{0.3}As$ well of width $L_z = 3$ nm. The horizontal bars give the rate of radiative recombination (the length corresponding to $10^{10}$ $s^{-1}$ is indicated). The three framed branches refer to Fig. 9.

$$\begin{aligned} H &= H_{\rm c.m.} + H_{\rm rel} + H_{\rm mix},\\ H_{\rm c.m.} &= \frac{\vec{P}^2}{2M} + \frac{1}{2}M\omega_{0,\rm c.m.}^2 R^2,\\ H_{\rm rel} &= \frac{\vec{p}^2}{2\mu} + \frac{1}{2}\mu\left(\omega_{0,\rm rel}^2 + \omega_{c,\rm rel}^2/4\right)r^2,\\ &\quad -H_{\rm int}(r) + \frac{1}{2}\gamma\omega_{c,\rm rel}L_{\rm rel},\\ H_{\rm mix} &= \omega_{c,\rm c.m.}\left(\vec{r}\times\vec{P}\right)_z + \mu\left(\omega_{0,e}^2 - \omega_{0,h}^2\right)\vec{r}\vec{R}. \end{aligned} \tag{20}$$

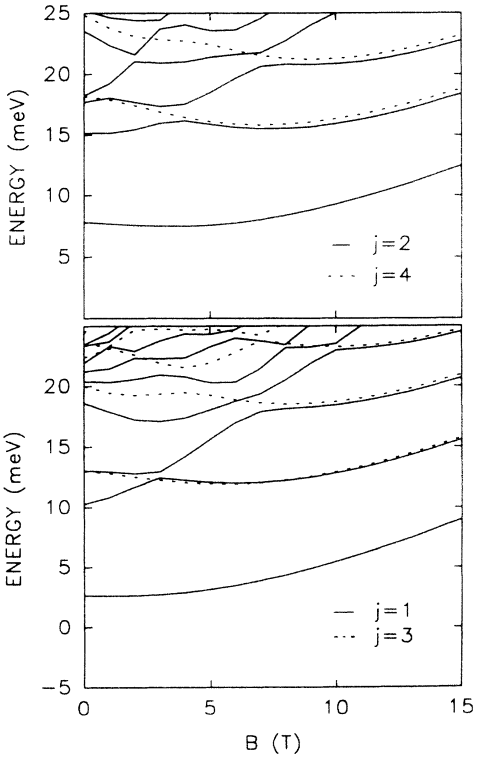


FIG. 7. Magnetic field dispersion of the nonradiative excitons ($j > 0$) for the quantum dot of Fig. 6.

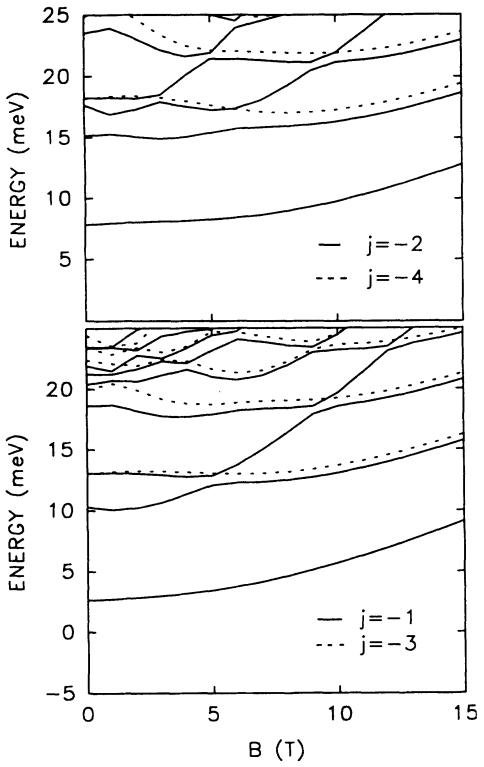


FIG. 8. Magnetic field dispersion of the nonradiative excitons ($j < 0$) for the quantum dot of Fig. 6.

$\vec{R} = (m_e\vec{r}_e + m_h\vec{r}_h)/M$ is the c.m. position vector (with conjugate momentum $\vec{P}$) and $\vec{r} = \vec{r}_e - \vec{r}_h$ the relative position vector (momentum $\vec{p}$). $M = m_e + m_h$, $\mu = m_e m_h/M$, $\gamma = (m_h - m_e)/M$, $\omega_{\mathrm{c,c.m.}} = eB/M$, $\omega^2_{0,\mathrm{rel}} = (m_h\omega^2_{0,e} + m_e\omega^2_{0,h})/M$, $\omega_{\mathrm{c,rel}} = eB/\mu$, $L_{\mathrm{rel}} = (\vec{r}\times\vec{p})_z$. $H_{\mathrm{c.m.}}$ represents a harmonic oscillator with an angular frequency given by $\omega^2_{0,\mathrm{c.m.}} = (m_e\omega^2_{0,e} + m_h\omega^2_{0,h})/M$. It is independent of magnetic field. $H_{\mathrm{rel}}$ depends on the lateral potential and magnetic field and contains the Coulomb potential and an angular momentum term. The latter decouples since it only acts on the angle of $\vec{r}$. Equation (20) suggests an expansion on a set of functions depending separately on $R$ and $r$. This approach indeed exhibits a faster convergency for weak lateral confinement.[32,33] However, the $r$ dependent basis functions are not analytical. This would be an important disadvantage in the present work, where the exciton wave functions are used to calculate the phonon scattering rates. We can give a rough assignment of the energy branches of Figs. 6–8 to a set of quantum numbers $(n_{\mathrm{c.m.}}, l_{\mathrm{c.m.}}, n_{\mathrm{rel}}, l_{\mathrm{rel}})$, always bearing in mind the mixing due to the term $H_{\mathrm{mix}}$. For the angular momentum quantum number holds: $j = l_e + l_h = l_{\mathrm{c.m.}} + l_{\mathrm{rel}}$. In this approximate way, the two lowest $j = 0$ branches correspond to (0,0,0,0) and (1,0,0,0) for all $B$, while the third branch evolves from (0,0,1,0) at zero-$B$ to (2,0,0,0) at high fields. For $j \neq 0$ the lowest branch corresponds to $(0,j,0,0)$. The magnetic field dispersion mainly arises from the magnetic field dependence of $H_{\mathrm{rel}}$. $H_{\mathrm{mix}}$ is responsible for the anticrossings.

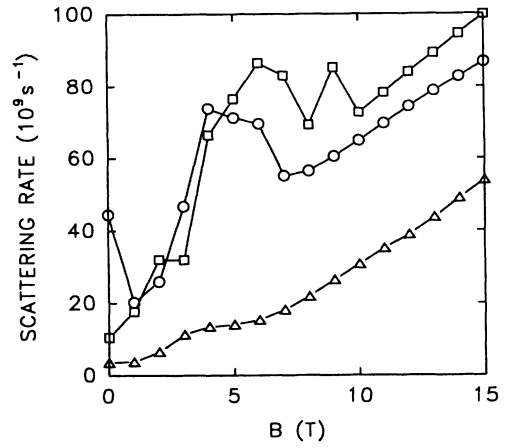


FIG. 9. Exciton-LA-phonon scattering rates in a quantum dot at zero temperature. The three curves correspond to the radiative initital states indicated in Fig. 6. The lines between the symbols are guides to the eye.

We now turn to scattering between the discrete exciton levels. As in the electron case, we consider the deformation potential interaction with bulk LA phonons in the Born approximation. The rate of scattering between a pair of exciton states is calculated from Eq. (7) where for $\psi_i$ and $\psi_f$ excitonic wave functions are introduced. Neglecting the nondiagonal terms in the valence band Hamiltonian, the operator for the heavy-hole exciton LA-phonon interaction,

$$W = \left(\frac{\hbar q}{2\rho_d c_s}\right)^{1/2}\left[De^{i\mathbf{q}\mathbf{r}_e} + \left(\frac{l+m}{2}\frac{(q_x^2+q_y^2)}{q^2} + m\frac{q_z^2}{q^2}\right)e^{i\mathbf{q}\cdot\mathbf{r}_h}\right], \qquad (21)$$

is the sum of the electron operator Eq. (8) and a hole operator which depends on the direction of propagation of the phonon.[7] For the valence band deformation potentials, we use $l = 2.7$ eV and $m = 8.7$ eV. Comparing Eqs. (18) with Eq. (21) we observe that the matrix elements of both $H_{\mathrm{int}}$ and $W$ are of the form given in Eq. (12), namely, harmonic exponentials in between single-particle harmonic oscillator functions. This is used in the numerical calculations. We calculate both matrix elements from a table of $G(Q,n,l,n',l')$.

Figure 9 shows the magnetic field dependence of the exciton-phonon scattering rates $\tau^{-1}$ for three different radiative excitons. The quantity $\tau^{-1}$ is the sum over the transition rates to all exciton states of energy below the initial state. This includes radiative as well as nonradiative excitons, there is no general selection rule. The scattering rates of the first excited radiative branch (triangles), for example, are dominated by transitions into states of $j = \pm 1$. For all three initial states, $\tau^{-1}$ increases with $B$. The reason for this increase is twofold. First, the magnetic field leads to a compression of the exciton wave function in the lateral directions and with that higher Fourier components become available to phonon scattering. Second, the energy separations between the initial

exciton states and the relevant final states decrease with increasing $B$. The pronounced oscillations of $\tau^{-1}$ for the two higher initial states are caused by variations in energy and wave function related to the anticrossing of the exciton states.

The magnetic field can accelerate exciton relaxation in quantum dots. This is an interesting result, in particular with respect to the magnetoptical properties. A rate equation analysis based on calculated exciton lifetimes shows that for the quantum dot discussed above excited state transitions are expected in luminescence at zero $B$, even at low excitation intensity.[7] This is in agreement with microscopic luminescence measurements on single quantum dots, where strong transitions blueshifted from the ground state have been observed.[8] From the present work we expect that luminescence arising from excited state transitions decreases in intensity compared to the ground state as a magnetic field is applied.

Let us finally consider the limit of zero lateral confinement, namely, the case of 2D magneto excitons. Is exciton relaxation between Landau levels similar to relaxation between the discrete states of quantum dots? For electrons there are similarites as shown in Sec. II B [Eq. (16)]. We have seen that a discrete electronic energy spectrum leads to a strong decrease in the electron-LA-phonon scattering rate $\tau^{-1}$ when the level separation exceeds a threshold depending on the smallest dot dimension. This also holds for excitons.[7] On the other hand, the energy spectrum of magnetoexcitons in 2D systems is continuous. This directly follows from Eq. (20), where the c.m. motion of the exciton is free for $\omega_{0,e} = \omega_{0,h} = 0$. This means that excitons can relax efficiently in small steps through the continuum of nonradiative states, even if the separation between the radiative levels (in the dipole approximation the states with zero c.m. momentum $\mathbf{P}$) is large. The relaxation dynamics of excitons in purely Landau quantized systems is, therefore, different from the one in quantum dots.

## IV. CONCLUSIONS

A theoretical study of electron-LA-phonon and exciton-LA-phonon scattering in fully quantized systems has been presented. In the Born approximation, we obtain comparable rates for electron scattering between states obtained by pure spatial quantization and by pure Landau quantization. Nevertheless, the two types of confinement are not equivalent. Starting from a dot with sizeable spatial quantization, increasing spatial confinement leads to a decreasing electron-phonon scattering rate, while an increasing magnetic field causes an increase in $\tau^{-1}$ followed by pronounced oscillations. In the same system, exciton relaxation by phonon emission become more efficient when a magnetic field is applied. For the exciton relaxation dynamics, spatial quantization is fundamentally different from pure Landau quantization.

## ACKNOWLEDGMENTS

I am pleased to thank G. Bastard for helpful discussions. The work has been partly supported by the Deutsche Forschungsgemeinschaft (SFB 348) and by a PROCOPE contract.

[1] For recent reviews see J. Y. Marzin, A. Izrael, and L. Birotheau, Solid-State Electron. **37**, 1091 (1994); R. Cingolani and R. Rinaldi, Riv. Nuovo Cimento **16**, 1 (1993).
[2] *Phonons in Semiconductor Nanostructures*, edited by J.-P. Leburton, J. Pascual, and C. Sotomayor Torres (Kluwer, Dordrecht, 1993).
[3] U. Bockelmann and G. Bastard, Phys. Rev. B **42**, 8947 (1990).
[4] H. Benisty, C. M. Sotomayor Torres, and C. Weisbuch, Phys. Rev. B **44**, 10 945 (1991).
[5] T. Inoshita and H. Sakaki, Phys. Rev. B **46**, 7260 (1992).
[6] U. Bockelmann and T. Egeler, Phys. Rev. B **46**, 15 574 (1992).
[7] U. Bockelmann, Phys. Rev. B **48**, 17 637 (1993).
[8] K. Brunner, U. Bockelmann, G. Abstreiter, M. Walther, G. Böhm, G. Tränkle, and G. Weimann, Phys. Rev. Lett. **69**, 3216 (1992); U. Bockelmann, K. Brunner, and G. Abstreiter, Solid-State Electron. **37**, 1109 (1994).
[9] M. Prasad and M. Singh, Phys. Rev. B **29**, 4308 (1984).
[10] O. Heinonen, P. L. Taylor, and S. M. Girvin, Phys. Rev. B **30**, 3016 (1984)
[11] S. Tamura and H. Kitagawa, Phys. Rev. B **40**, 8485 (1989).
[12] S. M. Badalian, U. Rössler, and M. Potemski, J. Phys. C **5**, 6719 (1993).
[13] G. Bastard, J. A. Brum, and R. Ferreira, in *Solid State Physics*, edited by H. Ehrenreich and D. Turnbull (Academic, New York, 1991), Vol. 44, p. 229.
[14] V. Fock, Z. Phys. **47**, 446 (1928).
[15] J. S. Gradshteyn and J. M. Ryzhik, *Tables of Integrals, Series and Products* (Academic, New York, 1965).
[16] S. Schmitt-Rink, D. A. B. Miller, and D. S. Chemla, Phys. Rev. B **35**, 8113 (1987).
[17] H. Rücker, E. Molinari, and P. Lugli, Phys. Rev. B **45**, 6747 (1992).
[18] F. Rossi, L. Rota, C. Bungaro, P. Lugli, and E. Molinari, Phys. Rev. B **47**, 1695 (1993).
[19] For an overview and further references see K. Misawa *et al.* and F. Henneberger *et al.* in *Optics of Semiconductor Nanostructures*, edited by F. Henneberger, S. Schmitt-Rink, and E. O. Göbel (Akademie Verlag, Berlin, 1993).
[20] K. Hirakawa and H. Sakaki, Appl. Phys. Lett. **49**, 889 (1986).
[21] Y. Okuyama and N. Tokuda, Phys. Rev. B **40**, 9744 (1989).
[22] P. J. Price, Ann. Phys. (N.Y.) **133**, 217 (1981).
[23] A. Gold, Z. Phys. B **74**, 53 (1989).
[24] T. Ando and Y. Uemura, J. Phys. Soc. Jpn. **36**, 959 (1974).
[25] S.-R. Eric Yang and L. J. Sham, Phys. Rev. Lett. **58**, 2598 (1987).
[26] G. E. W. Bauer and T. Ando, Phys. Rev. B **37**, 3130 (1988).

[27] T. Takagahara, Phys. Rev. B **47**, 4569 (1993).
[28] O. Akimoto and H. Hasegawa, J. Phys. Soc. Jpn. **22**, 181 (1967).
[29] R. L. Greene and K. K. Bajaj, Phys. Rev. B **31**, 6498 (1985).
[30] G. W. Bryant, Phys. Rev. B **37**, 8763 (1988).
[31] Y. Z. Hu, M. Lindberg, and S. W. Koch, Phys. Rev. B **42**, 1713 (1990).
[32] W. Que, Phys. Rev. B **45**, 11 036 (1992).
[33] V. Halonen, T. Chakraborty, and P. Pietiläinen, Phys. Rev. B **45**, 5980 (1992).
[34] B. Adolph, S. Glutsch, and F. Bechstedt, Phys. Rev. B **48**, 15 077 (1993).